การวิเคราะห์เงื่อนไขบังคับของงานประกอบสามมิติ

ชิต เหล่าวัฒนา [1]
มหาวิทยาลัยเทคโนโลยีพระจอมเกล้าธนบุรี

บทคัดย่อ

เครื่องจักรประกอบแบบยืดหยุ่นได้ (Flexible machine) อาจได้รับการปรับปรุงให้ดีขึ้น และด้านราคาถูกลง โดยการผ่อนคลายเงื่อนไขบังคับทางด้านความละเอียดและติดตั้งอุปกรณ์คอมพลาย-แอนซ์ (Compliance) ที่ปลายแขนงานประกอบ (Assembly Effector) เมื่อไม่นานมานี้อุปกรณ์เอสอาร์ซีซี (Spatial Remote Center of Compliance) สามารถใช้ในการประกอบชิ้นส่วนทรงเหลี่ยม (Prismatic Parts) อุปกรณ์นี้ถูกออกแบบบนพื้นฐานความเข้าใจและความเป็นไปได้ของลักษณะการสัมผัสของชิ้นงานที่สัมพันธ์กับตำแหน่งตั้งต้น และความไม่แน่นอนเชิงมุมกับชิ้นงานสัมผัส ลักษณะการสัมผัสของชิ้นงานเหล่านี้ถูกจัดในเชิงแผนภูมิโยงใยที่มีคุณสมบัติแบบเพ็ตดีเน็ท (Petri Net) อย่างไรก็ตามการควบคุมในช่วงทรานซิชั่น (Transition) ถูกบังคับจากคอมพลายแอนซ์ที่ตอบสนองต่อแรงสัมผัส (Contact Force) แทนที่จะใช้แรงที่วัดได้ (Sensed Forces) และใช้แผนงานควบคุมเหตุการณ์แบบไม่ต่อเนื่อง (Discrete Event) เส้นทางความเป็นไปได้ แผนภูมิโยงใย เงื่อนไขบังคับ (Constraints Network) จากจุดเริ่มต้นถึงจุดสุดท้ายของหมุดจตุรัส เส้นทางดังกล่าวใช้นิยามความสัมพันธ์ของคอมพลายแอนซ์สำหรับอุปกรณ์งานประกอบเชิงปฏิบัติได้ บทความนี้ยังได้วิจารณ์เทคนิคการออกแบบงานประกอบอื่นๆ ด้วย

---

[1] *ผู้ช่วยศาสตราจารย์ ศูนย์ปฏิบัติการพัฒนาหุ่นยนต์ภาคสนาม(ฟีโบ้)*

Analysis of Task Constraints for Three Dimensional Insertion

Djitt Laowattana [1]

King Mongkut's University of Technology Thonburi

Abstract

Flexible assembly machines may be improved and costs reduced by relaxing constraints on part fixturing accuracy and employing compliant devices in assembly effectors. An effector-mounted remote center compliance device that corrects for spatial misalignments of prismatic parts of general cross section has recently been demonstrated. This spatial RCC was designed by considering the possible assembly contact states given a range of initial position and orientation uncertainty between the mating parts. These contact states are arranged in a constraint network in the fashion of a Petri-Net controller. However, the control transitions are mediated by compliances reacting to contact forces rather than from force sensing and discrete event controller schemes. A path through the constraint network of a square peg and hole task is found from initial to final assembly states. This path defines a single compliance relationship that is realized with an practical assembly device. Extensions of this design technique to other assembly tasks are discussed.

Assistant Professor, Center of Operation *for Field Robotics Development (FIBO)*

1. Introduction

Assembly represents the largest area of direct and indirect cost in most manufactured products [Riley 83]. Assembly also consumes, on average, 50% of a product's in-plant cycle time. Automated assembly systems cannot effectively assemble parts featuring the three most ubiquitous assembly primitives: prismatic insertion, threaded fits and general path insertion. Such assembly tasks exhibit a high level of difficulty [Sturges 90]. Work by Whitney [82] has shown that the passive technique is far superior to active control schemes, in term of reliability and low cost for two dimensional-symmetric insertion, i.e., round pegs in round holes. A remote center of compliance (RCC) [Simunovic 75] was invented for such a purpose. Passive assembly means that parts mating routinely occurs without an active control scheme to correct for imprecise part/effector position. This assembly approach combines strategic open-loop part motion with compliance that responds to contact forces with desired motions. A strategy for inserting a chamfered, round peg into a round hole was established by Drake et.al. [77], and Whitney [82].

Using a pure positional control, the ensured success of peg insertion requires that the part clearance is not smaller than the accuracy and/or the repeatability of the manipulators and manufacturing jigs. Laboratory assembly robots which use force control often operate with inherent instability [Whitney 87], [Eppinger 92]. Active force-sensing control in the industrial environment is still far away from being practically applied at reasonable cost.

Recent work employing vibratory systems for insertion by Asada et. al [92] demonstrated two dimensional assembly of cable connectors. Optimum settings for the vibrator were obtained by Taguchi analysis to minimize friction and jamming. Work by Paetsch et.al. [13] focused on solving insertion tasks (square peg in hole) with a multifingered gripper. Paetsch implemented a force feedback strategy to ensure that intentional instability was employed. In this case, positional information was not accurate due to slipping at the fingers, and additional vision feedback was suggested. In general, active vibratory systems are slow and do not guarantee convergence towards the desired assembled state. An insertion task comprising a dual peg-n-hole was modeled by McCarragher and Asada [93] as a discrete event dynamic system using Petri nets. This "discrete event" controller moves towards the next desired contact while maintaining currently desired contacts. However, statically indeterminate states cannot be reliably detected. In particular, wedging must be avoided since recovery is difficult.

The conventional RCC has been shown to be unreliable for three dimensional, asymmetric insertion, e.g., square peg and hole with chamfer [Sturges and Laowattana 94]. In this kind of task, forces and moments are unlikely to pass through the vertical plane containing the compliance center of the device, and thus the torque and displacement about the vertical insertion axis cannot be ignored. This torque is resisted by the apparent stiffness of the compliant members (e.g. shear

pads) in the RCC, leaving the peg jammed against the chamfer. This jamming situation can occur at a point-surface contact between the bottom comer of the peg and either the area outside the chamfer, a point-surface contact on the chamfer, or a line-line contact between edges of the peg and hole. In addition, three dimensional virtual wedging [Sturges and Laowattana 92] is possible due to the three point contacts which cannot be avoided by the RCC [Sturges and Laowattana 1994].

Our previous work has also demonstrated that a compliant mechanism reacting at right angles to contact forces is sufficient for polygonal peg insertion. Such an "Orthogonal compliance" was designed through knowledge of the physics of the task and the effector as a system. This knowledge embodies relations among geometry of contacts, forces and moments. One result of this approach is a passive device using a single orthogonal compliant axis, to be described later. Although, this so-called Spatial Remote Center of Compliance (SRCC) is a passive device, we expect that active assembly devices will also benefit from the method developed in this paper. In the next section, we will describe a contact constraint analysis tool that can be used as a road map for designing compliances to accomplish assembly tasks.

2. Constraint Analysis in Two Dimensional Peg Insertion

A state network can be used to map contact states, one or more paths of which may lead to successful assembly. A state network may be comprised of a geometrical description of the contacts in assembly such as point-point, line-surface, etc., and the admissible transitions among them as shown in Fig. 1. At any node (N) in the network, these contacts are maintained by a set of physical and geometric constraints. The symbol (N) is used to represent the nodes. Thus, we define a Constraint Network as a state network that embodies physical models of contacts. Note that the transitions from one node to another is mediated by constraints at the contacts, whereas in the Petri net scheme [McCarragher and Asada 93] sensing and control govern those transitions. We will describe further the significance of using a constraint network to design compliant systems for assembly tasks. In this section, we show the similarity between the Petri net controller and a passive mechanism, the RCC, in two dimensional peg insertion. The advantage of passive mechanisms over active control will also be discussed.

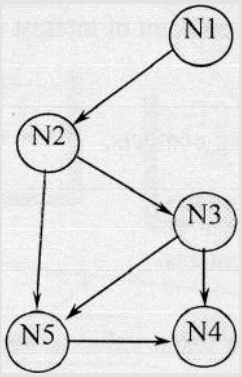

Figure 1 A state network

In the Petri net scheme, nodes represent either single or multiple contacts. A transition, symbolized by T, directs changes from one node to another. Each transition implies gain or loss of a single contact pair. The symbol ❑ denotes a discrete control that governs such a transition. Fig. 2 shows a such a transition between two nodes in the Petri net modeling of the two dimensional peg insertion problem.

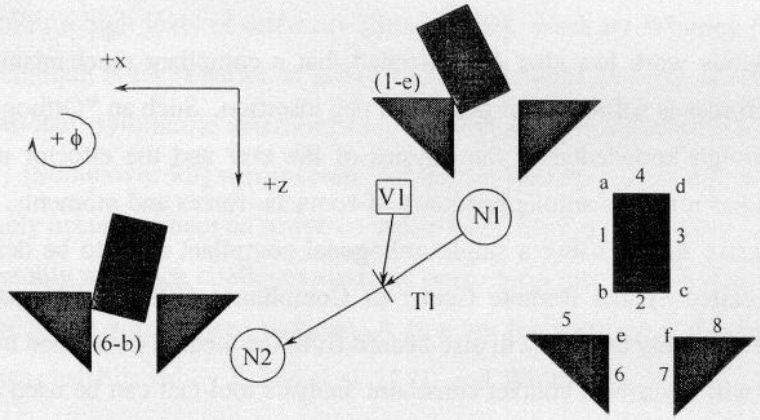

Figure 2 Partial Petri net for planar peg and hole problem
[After McCarragher and Asada 1993]

In this case, the input function defines the node N1, having the point-surface contact (1 -e). Before the Petri net controller can fire the transition T1, the node N1 must be active. This means that both a contact constraint at N1 is satisfied and the control V1 is enabled. The contact pairs resulting from the transition T1 is defined by an output function. If we represent each node by a P^{x1} vector where p is the number of contact pairs, firing a transition results in switching a token value between one and zero in the vector. The control V1 is determined by the generalized velocity $\dot{q}$ of the mating parts expressed by the associated pair of nodes. To find $\dot{q}$ for any transition, we may employ the admissible velocity $\overline{V}$ as derived by McCarragher and Asada [93]:

$$\overline{V} = D_i \dot{q} \qquad (1)$$

where D is the derivative with respect to the generalized coordinates of the normal distance from the corresponding surface to a given point of interest on the peg. Thus, there are three possible condition:s:

$\overline{V} = 0$, for maintaining contacts, (2.1)

$\overline{V} < 0$, for gaining contacts, (2.2)

$\overline{V} > 0$, for loosing contacts. (2.3)

Let $\Delta\Gamma_i$ be the change of the token value in the P^{x1} vector. Putting $\Delta\Gamma_i$ into (2.1) to (2.3) as 0, 1 and -1 respectively, we obtain a general form for the enabling condition:

$$\Delta\Gamma_i D_i \dot{q} < 0 \quad . \tag{3}$$

Similarly, the disabling condition is given by:

$$\Delta\Gamma_j D_j \dot{q} \geq 0, \ \forall j \neq i \quad . \tag{4}$$

Note that by solving a set of simultaneous linear inequalities Eqs.(3) and (4), and one equality constraint in Eq.(2.1), we may not obtain a unique solution for $\dot{q}$. Moreover, no feasible solution may exist. If there is more than one solution, the Max.-Min. strategy is used to determine the optimal velocity [See detail in McCarragher and Asada 93]. For example, let N1 and N2 in Fig. 2 represent the contact states l-e and 6-b respectively. Before firing the transition T1, eq. (2.1) is required for maintaining the contact (l-e). To enable the transition resulting in the (6-b) contact, we apply the enabling condition, eq.(3). The disabling condition, eq.(4) must also be applied to avoid the contacts (5-b) and (7-c). This disabling condition cannot be applied to the contact (2-f) since this would be inconsistent with the previous constraints, and therefore we are unable to guarantee the avoidance of the contact (2 -f). Although the Petri net gives a solution for peg motion in the desired directions (-x, +z, $+\phi$), it does not include a model of friction and sliding motions while the peg is making a line-line contact (1 – 6) with the hole. The absence of such states in the model and the difficulty of recognizing them in practice makes it difficult to determine the final contact state at N2. Also, jamming conditions must be considered at nodes having two point contacts.

The RCC can avoid such jamming conditions. The compliance center (●), shown in Fig. 3 is properly placed at a point where the ratio of forces and moments fall within the jamming diagram (see Fig. 4). We can easily show, with a force balance that the RCC also moves the peg in the same directions as found in the discrete event controller as follows:

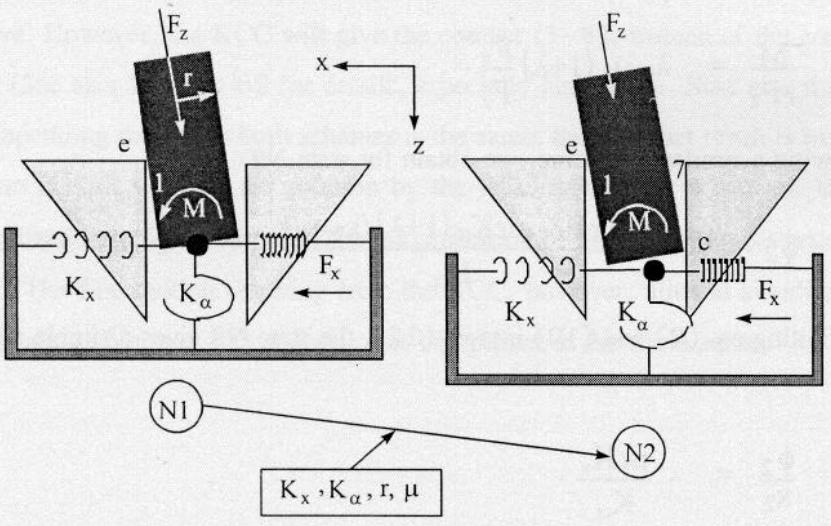

Figure 3 Model of forces and moments about the compliance center of an RCC

The forces and moments which can avoid jamming at the one-point contact (1 -e) [Whitney 82] are

$$\frac{F_x}{F_z} = -\frac{1}{\mu}, \text{ and} \quad (5)$$

$$\frac{M}{rF_z} = 2\lambda + 1, \quad (6)$$

where $\lambda = \frac{l}{2r\mu}$.

The terms F_x, F, M, r, and μ are lateral force, insertion force, moment, radius of the peg, insertion depth and coefficient of friction respectively. The moment and lateral force are support forces provided by angular and lateral springs (K_ϕ and K_x) in the RCC. We assume that both (x and ϕ) displacements start at zero and move to x_1 and ϕ_1:

$$F_x = K_x X_1, \text{ and} \quad (7)$$

$$M = K_\phi \phi_1 . \quad (8)$$

Substituting Eqs. (7) and (8) to Eqs.(5) and (6), we obtain the states X_1 and ϕ_1 at N1. Then:

$$x_1 = -\frac{F_z}{\mu K_x}, \text{ and} \quad (9)$$

$$\phi_1 = \frac{r(2\lambda+1)F_z}{K_\alpha} \quad (10)$$

During two point contacts(l-e and 7-c) shown in Fig. 3, the relation among M, F_x and F for the peg sliding into its hole is found from the jamming diagram in Fig. 4 to be:

$$\frac{M}{rF_z} = \lambda - \mu(1+\lambda)\frac{F_x}{F_z} . \quad (11)$$

Following a similar procedure, we obtain for state N2

$$\phi_2 - \phi_1 = \frac{\lambda r F_z + \mu r K_x (1+\lambda)(x_2-x_1)}{K_\alpha} \quad (12)$$

Substituting eq. (9) and (10) into eq.(12), the state N2 gives a simple relation between x_2 and ϕ_2 :

$$\frac{\phi_2}{x_2} = -\frac{\mu r K_x}{K_\alpha} . \quad (13)$$

Eq. (13) shows the compliances that govern the transition from node N1 to node N2. In general, we can determine states with positional uncertainty at each node (i.e. $x_i \pm \delta_{xi}$, $z_i \pm \delta_{zi}$, $\phi_i \pm \delta_{\phi i}$) by augmenting the given geometry of the peg and its mating hole. The symbol δ indicates the uncertainty in each dimension. In this case, there may be ranges of compliances required for each transition. For successful insertion, compliances governing all transitions in the state-network must be considered. The design values for compliances are determined by the intersection of such ranges.

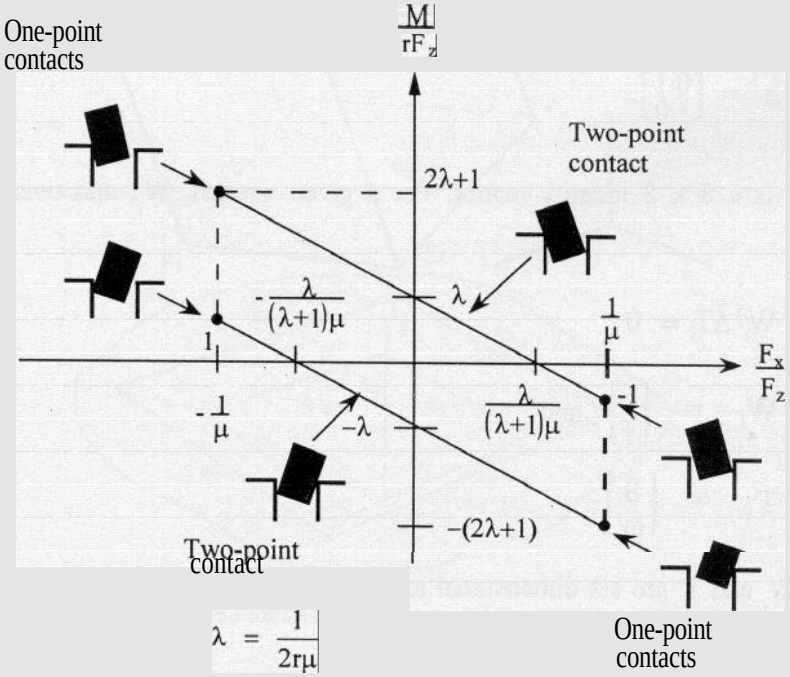

Figure 4 The Jamming Diagram [After Whitney 82]

For two dimensional peg insertion, the motion strategy is pushing downward (+z). Since the initial contact is (1 -e) resulting from downward motion, there will be displacement of the peg in -x direction. Thus, the directions of motion are (-x, +z, and + ϕ) as found by the Petri net approach above. However, the RCC will give the contact (1 - 6), instead of the contact (6-b) as the final state [See also Whitney 82 for details, especially his Fig. 8. Note also that although the direction of impending motion in both schemes is the same, the Petri net result is in the form of an accommodation control whereas the solution by the RCC is a stiffness control. In addition, the optimal generalized velocity is based on the maximization of the minimum distance to each contacting entity. The fine motion resulting from the RCC, however, aims at avoiding wedging and jamming constraints [Whitney 82] and may not be optimal in the same sense.

3. Modeling of contact states

Modeling of contact states in a quantitative form is important for reasoning about constraints and degrees of freedom among parts in assembly tasks. In this section, we will model contact states with screw theory [Ohwovoriole and Roth 1981], wherein screws serve as a wrench of constraint and a twist of freedom. When the virtual coefficient of two such reciprocal screws is zero, the contact between the two assembled parts is maintained while sliding may occur. The property of reciprocity is analytically given by an operator:

$$\tilde{\Delta} = \begin{bmatrix} 0 & I \\ I & 0 \end{bmatrix}, \tag{14}$$

where I is a 3 x 3 identity matrix. For a given wrench, W_i, and twist, T_i, we denote reciprocity by:

$$W_i^T \tilde{\Delta} T_i = 0, \tag{15}$$

$$\mathbf{W}_i = \begin{bmatrix} \tau \\ f \end{bmatrix}, \text{ and} \tag{16}$$

$$\mathbf{T}_i = \begin{bmatrix} \vartheta \\ \omega \end{bmatrix}. \tag{17}$$

where W_i and T_i are six dimensional axis coordinates of force and instantaneous velocity vectors, respectively.

A pair of screws is termed repelling when its virtual coefficient is positive. Repelling screws break contacts, between parts, i.e.:

$$W_i^T \tilde{\Delta} T_i > 0 . \tag{18}$$

Lines in space can be also modeled as screws by using Plücker coordinates $[\tilde{N}, \tilde{N}_o]$. $\tilde{N}$ are direction,cosines of a line which are not necessarily normalized. $\tilde{N}_o$ are the moments of the line such that if P is any point on this line:

$$\tilde{N}_o = P \times \tilde{N} \tag{19}$$

Contact constraints for bounding edges of polygonal parts such as a square peg and its mating hole are conveniently expressed in these coordinates. The development of jamming forces is greatly facilitated with this notation. We will begin enumerating all possible contacts between the square peg and hole. In the next section, one of many possible state networks for successful assembly will be constructed based on this enumeration.

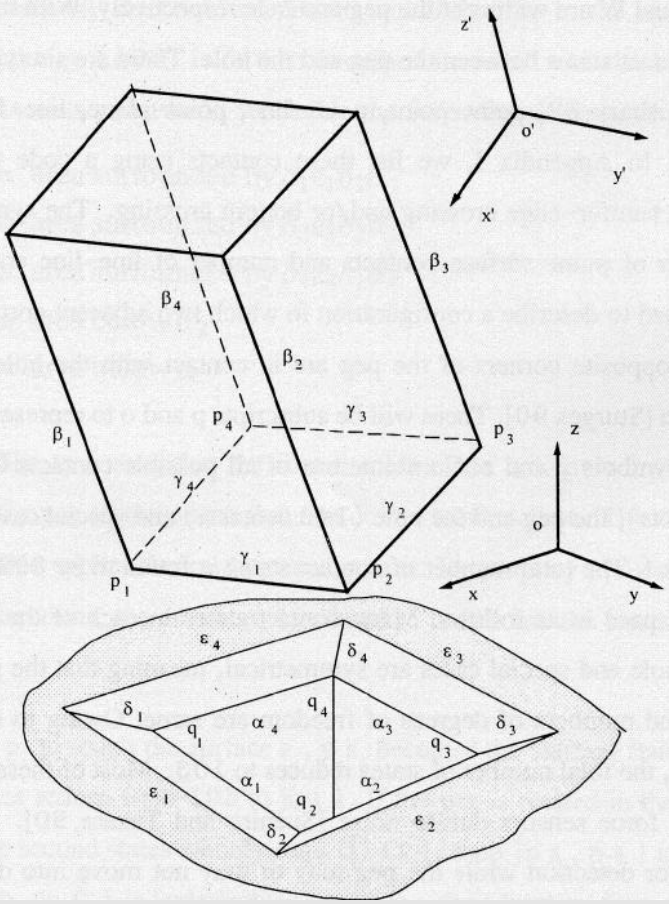

Figure 5 Feature definitions of a square peg and hole

Figure 5 shows a set of feature definitions for the square peg and hole. Designations for bounding edges and forces have been attached. A reference frame for the peg is denoted with primes ($'$). The four side edges are described by line segments β_i' (i= 1, .., 4); the four bottom edges by line segments γ_i' (i = 1, . ., 4). 0' is the origin of reference coordinates for the peg which is attached to the first bottom comer, p,. For the square hole, the four top inner edges are described by line segment α_i (i = 1, . . , 4). The outer edges of the chamfer are denoted by line segment ε_i (i = 1, .., 4) and the four chamfer comers by line segment δ_i (i = 1, .., 4). It is assumed that the inner edges lie mutually normal to lines α_i. 0 is the origin of reference coordinates for the hole which is attached to the first inside corner, q,. In addition, each chamfer surface is defined by a point e_i in the plane which contains lines α_i and ε_i. Examples of feature definition defined in coordinates are:

$$\beta_2' = (0\ 0\ 0, w\ 0\ 0), \text{ and} \qquad (20)$$

$$\alpha_2 = (0\ 0\ 1, 0\ 0\text{-}W). \qquad (21)$$

The terms w and W are widths of the peg and hole respectively. With the definitions above, we will enumerate contact states between the peg and the hole. There are six types of contacts to be considered, viz.: [Salisbury 82] point-point, point-line, point-plane, line-line, line-plane and plane-plane contacts. In Appendix I, we list these contacts using a code to indicate multiple contacts that involve chamfer-edge crossing and/or bottom crossing. The symbols xx.y.z refer to contact types, number of point-surface contacts and number of line-line contacts, respectively. The term "Para" is used to describe a configuration in which two adjacent corners of the peg touch the hole. When two opposite corners of the peg are in contact with the hole, we refer it as the "Ortho" configuration [Sturges 90]. There will be subscripts p and o to represent the para and ortho configuration at the symbols y and z. Combinations of all possible contacts between peg and the chamfers (2 3 6 contacts), the peg and the hole (14 3 contacts) and special cases (20 contacts) are tabulated in Appendix I. The total number of contact states is found to be 399. We will find ways to truncate this state space in as follows. Many contact states in each of the three categories i.e. peg-chamfers, peg-hole and special cases are symmetrical, meaning that the peg is constrained in the similar manner and numbers of degrees of freedom are same. Owing to the symmetry of the parts to be assembled, the total number of states reduces to 10 3. Most of these states are at present difficult to detect by force sensors due to noise [Suehiro and Takase 90]. An extra motion is sometimes required for detection while the peg may or may not move into desired directions for completing the insertion.

Using the definitions given, the lateral and angular displacements of the peg with respect to applied forces and moments for successful assembly can be determined as in Eq. 12 & 13 above. These relationships will help us devise insertion strategies, some of which may be performed by passive mechanisms. For example, an RCC is modeled as a non-linear, planar compliance. With this device guiding the motion of a cylindrical peg, an insertion path at the top of the peg can be simply a straight line, while the RCC reacts to contacts to guide the peg. It is necessary that the RCC follows a path (consisting of a series of contacts) that avoids wedging and jamming conditions. Suitable forces and moments, satisfying constraints at each contact, must be applied to avoid jamming. Fig. 4 shows such constraints on one-point and two point contacts for the planar case [See also Whitney 82].

The same approach may be used in devising strategies/mechanisms for prismatic insertion, e.g., a motion sequence that predicts certain contacts occurring in order and that changes to a new direction after each contact has occurred. Alternatively, one could use an RCC to correct θ and ϕ errors, and at the same time, to correct for azimuth misalignments by deliberately rotating about the z-axis. To know in which direction to rotate, we need to pre-orient the peg. Assuming that the maximum angular uncertainty in azimuth is equal to $\pm\psi$, the angle for pre-orientation is just ψ

(either sign). The assembly direction in azimuth would then be in the opposite direction. This ***Azimuth Rotation Strategy*** (ARS) is further described in detail with the help of a contact state network. To construct a state-network, we define the following parameters as shown in Fig. 5:

$s_1 \equiv$ area surrounded by $\delta_1\varepsilon_1\delta_2\alpha_1$
$s_2 \equiv$ area surrounded by $\delta_2\varepsilon_2\delta_3\alpha_2$
$s_4 \equiv$ area surrounded by $\delta_4\varepsilon_4\delta_1\alpha_4$
$a_2 \equiv$ area below α_2
$a_3 \equiv$ area below α_3

We would like to ensure that the first contact made is known ***a priori.*** One strategy to ensure this is to tilt the peg slightly such that one corner touches first. The ARS for pre-orienting the azimuth axis is also applicable for the x and y axes. By properly pre-orienting the peg in the $+\theta$, $-\phi$, and $+\psi$ directions, the corner p_1 can be tilted to become the lowest point of the peg, as shown in Fig. 5.

In lowering p_1 to touch the surface s_1, p_1s_1 becomes the starting state. With the ARS, the possible starting states reduce from 103 to just 1. If the peg is rotated in the $-\psi$ direction, there will be three possible second states namely state $\{\beta_1\alpha_1\}$, state $\{p_1s_1, p_4s_4\}$ and state $\{p1 \text{ on } \delta1\}$. Note that the state $\{p_1 \text{ on } \delta_1\}$ is undesirable since it is a dead location from which the peg cannot move further. All other states beyond this level can be derived similarly, i.e. rotating in the $-\psi$ direction in combination with other motions. Fig. 6 shows a state network reaching a number of subgoal states. Due to limited space in this figure, gain or loss of more than one contact at time is shown. We can always decompose the node to represent just one contact change. At each of the subgoal states shown, all corners of the peg are below the α_1 lines. Reliable insertion is assured when the square peg is in the subgoal state since parts of the geometry of the peg and hole have been matched and all of the forces which could cause jamming are pointing towards the assembly direction. However, the possibility of additional wedging conditions still exists if a residual torque, generated by the azimuth stiffness, exerts substantial forces at the side wall contacts.

Note that this state network is derived by essentially fixing θ and ϕ. Some states can be skipped if the magnitude of θ or ϕ reduces during the transition. Likewise, if θ or ϕ can increase, there will be more undesired states in the network. Since an RCC is expected to be a part of this new strategy, θ and ϕ cannot grow, and this state network will conservatively represent the actual contacts. Further insertion after either of the subgoal states is reached still depends on a suitable pitch to avoid wedging and jamming. Here, pitch refers to the ratio between simultaneous translational and rotational displacement in a single motion.

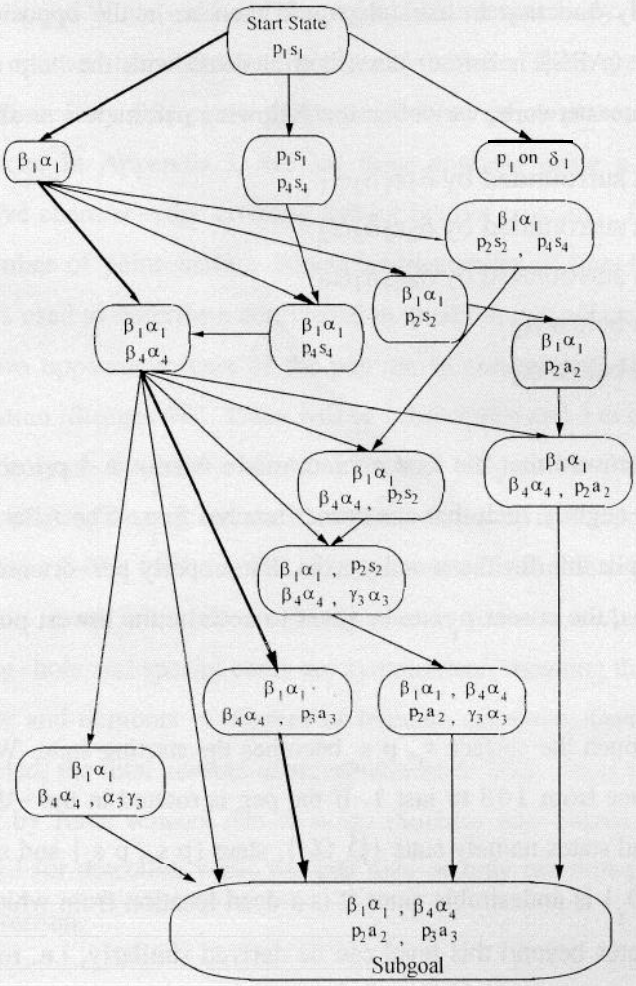

Figure 6 A State Network by Rotating Ψ

The state network in Fig. 6 can be further truncated by adding constraints. For example, in the next section, we will derive the constraints to insure that another point-surface contact on the chamfer does not occur while the peg is moving from the first point surface contact, $p_1 s_1$, to the first line-line contact, $\beta_1 \alpha_1$. Generally, the contact states progress from $p_1 s_1$ to the groups described below. The principal states are underlined:

- Group 1. One "β" line-line contact : $\{\beta_1 \alpha_1\}$, $\{\beta_1 \alpha_1$, one or two or three point contacts from combination of the set $p_2 s_2$, $p_3 s_3$, and $p_4 s_4\}$
- Group 2. Two "β" line-line contact : $\{\beta_1 \alpha_1, \beta_4 \alpha_4\}$, $\{\alpha_1 \beta_1, \beta_4 \alpha_4$, or one or two point or line-line contacts from combination of the set $p_2 s_2$, $p_3 s_3$, $\gamma_1 \alpha_2$ and $\gamma_3 \alpha_3\}$
- Group 3. Two "β" line-line contacts and one point contact in the hole: $\{\beta_1 \alpha_1, \beta_4 \alpha_4$, $p_2 a_2$ or $p_3 a_3\}$, $\{\alpha_1 \beta_1, \beta_4 \alpha_4, p_2 a_2$ or $p_3 a_3, \gamma_2 \alpha_2$ or $\gamma_3 \alpha_3$ or $p_3 s_3\}$

- **Group 4.** Two "β" line-line contacts and two point contacts in the hole: {$\beta_1 \alpha_1, \beta_4 \alpha_4$, $p_2 a_2$ and $p_3 a_3$}

In general, there are two approaches to reaching the subgoal states through the groups listed above.

3.1 A motion strategy using active movement with or without the RCC

In the literature, an active motion strategy with the RCC has not yet been reported, but success in the three dimensional peg insertion tasks would be possible if the motion strategy follows the state network of Fig. 6. The RCC corrects planar errors (x and ϕ) whereas an active movement by a robot aims at reducing the error in ψ. Active movement alone without passive mechanisms, i.e., force control guided assembly, may lead to instability [Eppinger and Seering 92]. Another active motion strategy is generated by the "magic wrist" [Oh, Hollis and Salcudean 93], a magnetically levitated mechanism that can be used to simulate the functions of RCC in axisymmetric two dimensional peg insertion tasks at high bandwidth.

In active systems, it is possible for the robot to generate a constant torque. However, without suitable pitches for ψ correction, the peg could rest at a dead contact state.

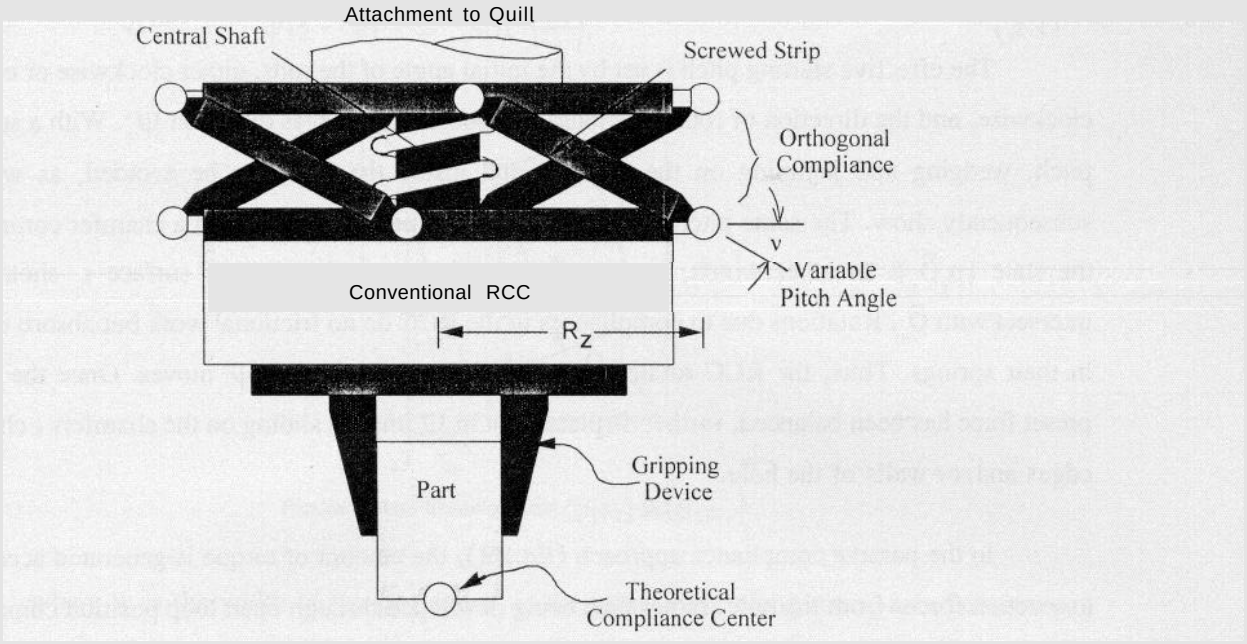

Figure 7 Spatial Remote Center of Compliance

3.2 Passive movement by the SRCC

As shown in Fig. 7, the SRCC consists of a conventional RCC in series with a mechanism for correcting errors in the azimuth angle (called a z-corrector). The RCC corrects the lateral and angular errors in the x and y axes while the z-corrector corrects the azimuth error. One type of the

z-corrector, depicted here, is a skewed rod-mechanism which converts linear motion into angular motion or vice versa. Each rod is connected to a pair of plates by ball joints. Such joints can accommodate spatial motion of the rod while its ends are constrained to move in planes. The top plate is aligned parallel with the bottom plate by a central shaft. The pitch of the z-corrector can be varied by adjusting the initial angle of the rods. The spring inside can also be adjusted to give a preset force. The preset force helps maintain the initial position of the z-corrector when there is no contact. This configuration of the z-corrector exhibits the low frictional internal resistance to motion necessary to assure sliding contacts between the mating parts.

Using the ARS, the peg is initially oriented to $\theta_1 \pm \delta_{\theta 1}$, $\phi_1 \pm \delta_{\phi 1}$, and $\psi_1 \pm \delta_{\psi 1}$ such that the peg tilts as shown in Fig. 3. To successfully insert the peg into its hole, all these initial errors must be corrected by the SRCC. The SRCC simultaneously corrects both the error in the vertical planes (x, ϕ, and y, θ) and generates the necessary torque for W-rotation to urge the peg to follow the state network. This torque also avoids wedging, jamming and dead locations, e.g., state $\{p_1$ on $\delta_1\}$.

When the z-corrector is acted on by a thrust force due to contacts between the peg and hole, it responds by providing a torque and rotation in a direction which is orthogonal to the force:

$$\text{Torque} = \text{Pitch} \times (\text{thrust force} \cdot \text{preset force}) . \qquad (22)$$

The effective starting pitch is set by the initial angle of the rods, either clockwise or counter clockwise, and the direction of rotation should be opposite to the bias direction ψ_1. With a suitable pitch, wedging and jamming on the chamfer and inside the hole can be avoided, as we will subsequently show. The same pitch should not allow the peg to get stuck on a chamfer corner, i.e. the state $\{p_1 \delta_1\}$. In other words, the locus of points p_1 on the chamfer surface s_1 should not intersect with δ_1. Rotations due to compliances in the RCC do no frictional work but absorb energy in their springs. Thus, the RCC rotates θ and ϕ fractionally before ψ moves. Once the initial preset force has been balanced, further displacement in ψ implies sliding on the chamfers , chamfer edges and/or walls of the hole.

In the passive compliance approach (Eq.22), the amount of torque is generated according to reaction forces from the hole, rather than being developed through open loop position commands as mentioned in 3.1 above. When the peg slides into the hole, arriving at one of the subgoal states, the reaction force reduces and so does the torque of the z-corrector.

4. Derivation of Contact State Constraints

We now find the constraints that govern contact states in the state network obtained in the previous section. From Fig. 6, there are several successful assembly paths. We will show constraint equations for the following path: $\{p_1s_1\}\rightarrow\{\beta_1\alpha_1\}\rightarrow\{\beta_1\alpha_1, \beta_4\alpha_4\}\rightarrow\{\beta_1\alpha_1, \beta_4\alpha_4, p_3a_3\}$. The nodes corresponding to this path are N1, N2, N3 and N4 respectively. After N4, the peg will reach at a subgoal state: $\{\beta_1\alpha_1, \beta_4\alpha_4, p_2a_2, p_3a_3\}$. These constraints can be classified according to physical contact modality (viz.: point-surface, point-line, and line-line), dead point avoidance and jamming avoidance due to friction. Relationships for physical contact will be given by Eq.(26), Eq.(31) through Eq.(45), and Eq.(48) through Eq.(50). Constraints governing dead point avoidance will be shown in Eq.(2 3) and Eq. (2 7) through Eq. (2 9). Jamming avoidance will be given by Eq.(30), Eq.(46) and Eq.(47).

Using the ARS, the state $\{p_1s_1\}$ is initially assumed. During the state transition from to $\{p_1s_1\}$ $\{\beta_1\alpha_1\}$ it is possible that other point-surface contacts may occur and peg corner p_1 may rest in chamfer corner $\delta 1$. The peg can be constrained to avoid such situations as follows. Fig. 8 shows the starting state $\{p_1s_1\}$ before moving to $\{\beta_1\alpha_1\}$. The maximum possible angular displacement $\Delta\psi$ can be approximately obtained from:

$$\Delta\psi = \psi_{12} - \psi_1 \leq \sin^{-1}\left(\frac{x_1}{w}\right) \qquad (23)$$

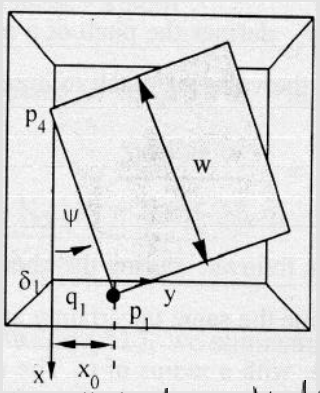

Figure 8 State transition from $\{p_1s_1\}$ to $\{\beta_1\alpha_1\}$

where w is the width of the peg and x_1 is the initial error along the x-axis between peg corner p_1 and hole corner q_1. The subscripts also represent the node number. The subscript 12 indicates the intermediate state between N1 and N2, viz., position and orientation corresponding to $\{p_1\alpha_1\}$. Note that the origins of the peg and hole frames reside at the corner p_1 and the corner q, respectively. Since there is no active force in the y direction, there is no change in θ:

$$\theta_2 = \theta_{12} = \theta_1 \qquad (24)$$

It is required at this stage of the assembly process that θ_1 be greater than zero such that the states $\{p_2 s_2\}$ and $\{p_3 s_3\}$ can be avoided. In addition, the states $\{p_3 s_3\}$ and $\{p_4 s_4\}$ can be avoided by initially setting $\phi_1 \geq 0$. Assume that the peg is now held by the RCC. Whitney [82] has shown that the change in ϕ during a point-surface contact is given by:

$$\phi_{12} = \phi_1 + \frac{K_x \left(\frac{z_1}{\tan \eta}\right) (L_g \mathbf{B} - r \mathbf{A})}{(K_x L_g^2 + K_\phi) \mathbf{B} - K_x L_g r \mathbf{A}}, \qquad (25)$$

where

$$\mathbf{A} = \cos \eta + \mu \sin \eta,$$
$$\mathbf{B} = \sin \eta + \mu \cos \eta.$$

For an RCC, the distance between the peg tip to the compliance center L_g is zero. The term r is approximately $0.5w$ and η is the chamfer angle. The vertical distance z_1 is measured from the state $\{p_1 s_1\}$, and to the state $\{p_1 \alpha_1\}$. ϕ_{12} is at the state $\{p_1 \alpha_1\}$. This state is between the point-surface and the line-line contacts. Note that both θ_1 and ϕ_1 can be made more than zero by orienting the peg through the ARS. With some manipulation, we obtain a constraint in ϕ during this transition:

$$\$_{12} \geq \frac{K_x z_1 w \mathbf{A}}{2 K_\phi \mathbf{B} \tan \eta}. \qquad (26)$$

The ratio between z_1 and ψ_{12} defines the pitch of a motion during chamfer crossing. Our previous work [94] has determined the value of pitch to avoid the dead location $\{p_1 \delta_1\}$ to be

$$\text{Pitch} = \frac{z_1}{\psi_{12}} = \frac{w \sin \eta \cot \zeta}{2}. \qquad (27)$$

Angle ζ can be obtained as follows: during the change from the state $\{p_1 s_1\}$ to the state $\{p_1 \alpha_1\}$ as shown in Fig 9, we assume the same uncertainty at both the point p_1 and the location of the hole, q_1, represented by a circle, with a radius of r_u. The uncertainty circle of q_1 intersects α_1 at I_1. From I_1, a line is drawn, tangential to the uncertainty circle of p_1. The line with maximum pitch, i.e., $I_1 p_u$ (the longest one), is selected. Let ζ be the angle $I_1 p_u$ makes with the perpendicular to α_1. Angle ζ can be graphically computed. Pitch of eq. (27) is found by ratio of the linear and angular displacement from:

$$\text{Linear displacement} = (I_1 p_u) \cos \zeta \sin \eta, \qquad (28)$$

and

$$\text{Angular displacement} = \frac{2 (I_1 p_u) \sin \zeta}{w}. \qquad (29)$$

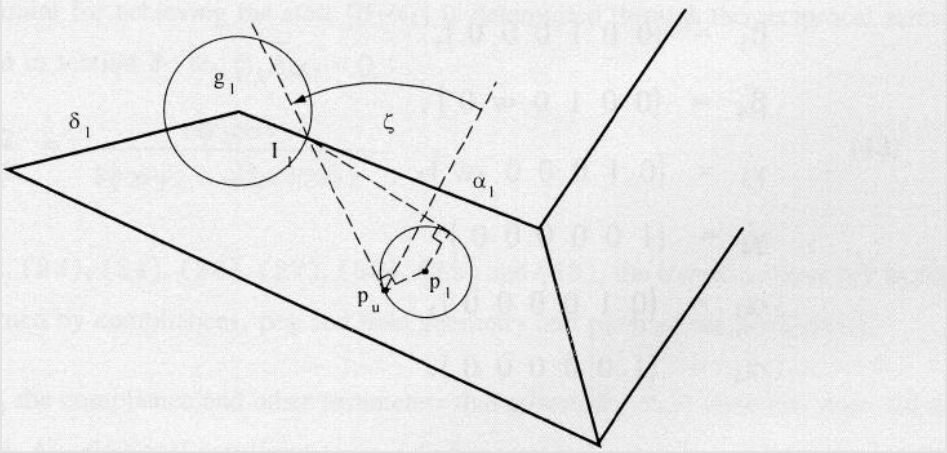

Figure 9 Selected Path(P_{u1}) on the Chamfer

Eq. (2 7) is a necessary condition to be satisfied for successful chamfer crossing. However, coloumb friction represented by μ will also determine whether or not p_1 can actually slide on the chamfer surface. The limiting value of μ as determined in [Sturges and Laowattana 94] is

$$\mu = \frac{2\,(\text{Pitch})\,c\eta}{w\sqrt{a^2 + b^2}}, \qquad (30)$$

where

$$a = (s\psi c\phi + s\theta s\psi s\phi + c\,\psi c\theta), \text{ and}$$

$$b = (c\psi c\phi + s\theta s\psi s\phi - s\psi c\theta).$$

From the relationships expressed in eq.(10) of Whitney [82], we find the ϕ_2 during a line-line contact:

$$\$2 = \frac{K_\phi \phi_{12} + K_x (z_2 + \mu r)}{K_\phi + z_2 K_x (z_2 + \mu r)}. \qquad (31)$$

By substituting Eq. (26) into Eq.(31), we eliminate ϕ_{12} and find the constraint in ϕ at N2 is

$$\phi_2 = \frac{K_x z_1 w\mathbf{A} - K_x (z_2 + \mu r)\,(2\mathbf{B}\tan\eta)}{(2\mathbf{B}\tan\eta)\,[K_\phi + z_2 K_x (z_2 + yr)]}. \qquad (32)$$

The geometric constraints for line-line contacts can be derived by using the following definitions of lines in Plucker coordinates:

$$\beta_1' = (0\ 0\ 1\ 0\ 0\ 0), \quad (33)$$

$$\beta_4' = (0\ 0\ 1\ 0\ w\ 0), \quad (34)$$

$$\gamma_3' = (0\ 1\ 0\ 0\ 0\ -w), \quad (35)$$

$$\gamma_4' = (1\ 0\ 0\ 0\ 0\ 0), \quad (36)$$

$$\alpha_1 = (0\ 1\ 0\ 0\ 0\ 0), \quad (37)$$

$$\alpha_4 = (1\ 0\ 0\ 0\ 0\ 0), \quad (38)$$

Angle β_1 with respect to the hole frame, can be determined by using a transformation matrix D_h^p between the peg frame (prior ned) and the hole frame:

$$\beta_1 = D_h^p \beta_1', \quad (39)$$

where

$$D_h^p = \begin{bmatrix} d_{11} & d_{12} & d_{13} & x_o \\ d_{21} & d_{22} & d_{23} & y_o \\ d_{31} & d_{32} & d_{33} & z_o \\ 0 & 0 & 0 & 1 \end{bmatrix}. \quad (40)$$

Elements d_{xy} in the rotation matrix are:

$$R_h^p = \begin{bmatrix} c\psi c\phi & s\theta c\psi s\phi - s\psi c\theta & s\theta s\psi + c\theta c\psi s\phi \\ s\psi c\phi & s\theta s\psi s\phi + c\psi c\theta & c\theta s\psi s\phi - s\theta c\psi \\ -s\phi & c\psi s\theta & c\phi c\theta \end{bmatrix}, \quad (41a)$$

The terms x_o, y_o and z_o indicate the distances between the origins of the hole and the peg frames along the x-axis, y-axis and the z-axis respectively. For small values of θ, ϕ and ψ, R can be approximately as:

$$R_h^p = \begin{bmatrix} 1 & -\psi & \phi \\ \psi & 1 & -\theta \\ -\phi & \theta & 1 \end{bmatrix}. \quad (41b)$$

At state N2, the subscript o in Eq. (40) becomes 2. Substituting eq. (4 0) into eq. (3 9), we obtain β_1 :

$$\beta_1 = \begin{pmatrix} d_{13} \\ d_{23} \\ d_{33} \\ y_2 d_{33} - z_o d_{23} \\ z_2 d_{13} - x_o d_{33} \\ x_2 d_{23} - y_o d_{13} \end{pmatrix} \quad (42)$$

The constraint for achieving the state $\{\beta_1 a_1\}$ is determined through the reciprocal screw system, mentioned in section 3 viz.: $\beta_1 \tilde{\Delta}\alpha_1 = 0$:

$$\frac{z_2}{x_2} = \frac{c\phi_2 c\theta_2}{s\phi_2 s\psi_2 + c\theta_2 c\psi_2 s\phi_2}. \qquad (43)$$

From Eqs. (23), (24), (26), (27), (30), (32) and (43), the transition from N1 to N2 is expressly governed by compliances, peg and hole geometry and pitch of the z-corrector.

Similarly, the compliance and other parameters that govern the state transition from **N2 to** N3 can be derived. An additional constraint to eq. (43) is required, viz.: the reciprocal screw for the state $\{\beta_4\alpha_4\}$. Following a similar procedure according to Eq. (3 9) through Eq. (4 3), we obtain:

$$\mathbf{x3} = \frac{y_3(s\theta_3 s\psi_3 + c\theta_3 c\psi_3 s\phi_3) - w(c\phi_3 s\theta_3)}{c\theta_3 s\psi_3 s\phi_3 - s\theta_3 c\psi_3} \qquad (44)$$

To maintain the state $\{\beta_1 a_1, \beta_4\alpha_4\}$, the constraint Eq. (4 3) and (44) must be satisfied simultaneously. Note that the subscripts in Eq.(43) change from 2 to 3 since we are considering states at N3. The state $\{\gamma_4\alpha_4\}$ must also be avoided before the second line-line contact occurs. The repelling screw system, $\gamma_4\tilde{\Delta}\alpha_4 > 0$, expressing this constraint gives:

$$\frac{z_0}{x_0} > -\frac{\tan\phi}{c\psi} \qquad (45)$$

Although at this stage, the peg has successfully slid on the chamfer into the hole, it is still possible for the peg to jam while making two line-line contacts. In general, we can determine a moment M required to overcome frictional forces at such multiple contacts as

$$M = \frac{f_1}{\mu} \times \frac{w}{2}, \qquad (46)$$

where f_i are contact forces. An example of four point contacts are shown in Fig 10. Multiplying Eq. (46) by μ and dividing both sides by the friction force, we found the upper bound of pitch needed to avoid jamming of multiple contacts inside the hole or at the chamfer edges α_i to be

$$\text{Pitch} = \frac{z_3 - z_2}{\psi_3 - \psi_2} < \frac{w}{2\mu}. \qquad (47)$$

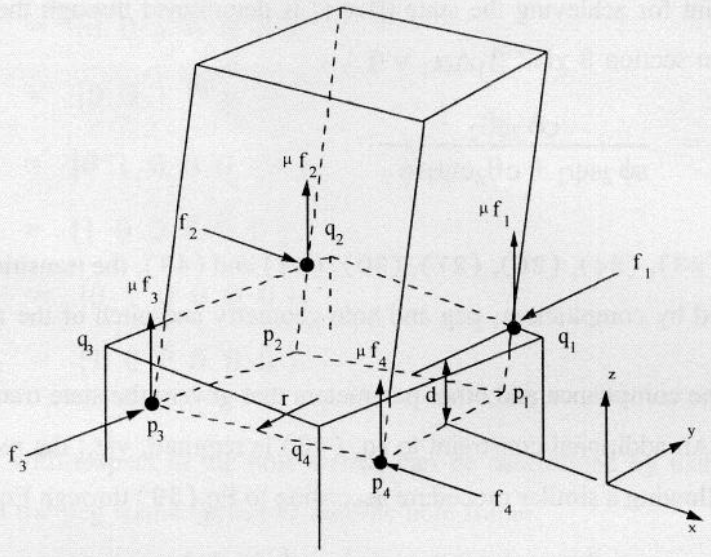

Figure ID Four point contact at onset of jamming

Eq. (44) through Eq. (47) show that the transition from N2 to N3 is governed by peg and hole geometry and pitch of the z-corrector. The compliance of the RCC also governs the state transition as follows:

$$\phi_3 = \frac{K_\phi \phi_2 + K_x (z_3 + \mu r)}{K_\phi + z_3 K_x (z_3 + \mu r)}, \text{ and} \quad (48)$$

$$\theta_3 = \frac{K_\theta \theta_2 - K_y (z_3 + \mu r)}{K_\theta + z_3 K_y (z_3 + \mu r)} \quad (49)$$

The state $\{\gamma_3 \alpha_3\}$ must be avoided such that a transition can be made to the state $\{\beta_1 \alpha_1, \beta_4 \alpha_4, p_3 a_3\}$. The repelling system, $\gamma_3 \tilde{\Delta} \alpha_3 > 0$, yields the following constraint at N4:

$$z_4(s\theta_4 c\psi_4 s\phi_4 - s\psi_4 c\theta_4) - (x_4 - W_d(\phi_4 s\theta_4 + W_c\theta_4 s\psi_4 s\phi_4 - s\theta_4 c\psi_4) > 0. \quad (50)$$

Another repelling screw: $\gamma_2 \Delta \alpha_2 > 0$ is required before the peg can reach the subgoal state $\{\beta_1 \alpha_1, \beta_4 \alpha_4, p_2 a_2, p_3 a_3\}$.

From Eq. (26), (27), (30), (32), (43), (44), (45), (47), (48) and (49), we can determine the range of compliance in each transition given that the six parameters (x, y, z, θ, ϕ and ψ) in each node (N1 to N4) and geometry of the peg and its hole is specified. The parameters at N4 must also satisfy Eq.(50) in order to avoid jamming while α lines cross.

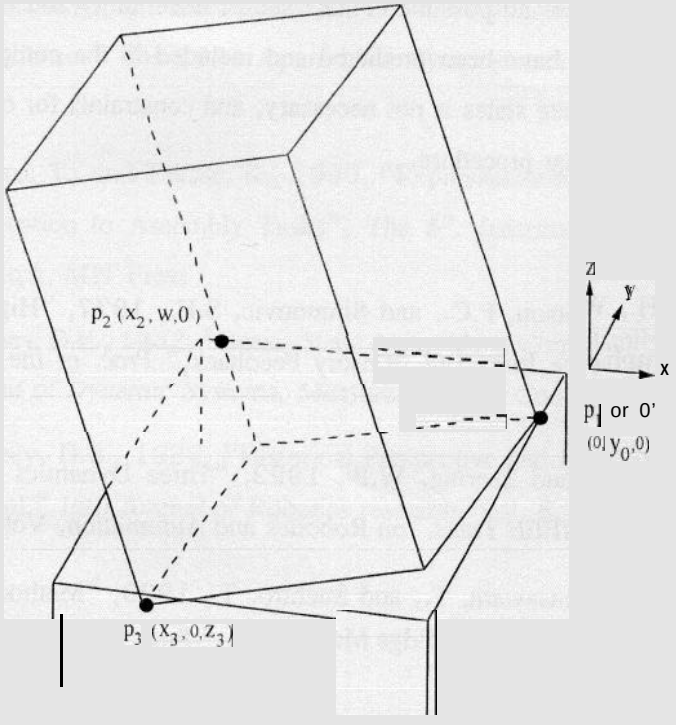

Figure 11 Ortho configuration at onset of wedging

5. Conclusion

In this paper, all possible contact states in an insertion task of a square peg and hole are exhaustively enumerated based on given a range of initial position and orientation uncertainty between the mating parts. A state network is then constructed by connecting nodes that change one state at a time. Parts of this state-network are found to be successful insertion paths. One of those possible paths requires a special type of compliance for eliminating the error in azimuth angle. This so-called orthogonal compliance can be realized with a mechanism. The mechanism will react to a given vertical contact forces by moving in an orthogonal direction, resulting in a twisting motion about the vertical axis. By combining such a mechanism with an axisymmetric (planar) RCC, we obtain a spatial compliance that is able to guide a square peg successfully into its mating square hole from an uncertain initial state to a final assembled state. A prototype of this Spatial Remote Center of Compliance (SRCC) also corrects for spatial misalignments of prismatic parts of general cross section.

The constraints governing the state transitions along a path toward insertion are derived from reciprocal and repelling screw systems. These constraints, resulting from engineered compliances, part geometry and surface friction, mediate the state transitions; whereas, in a Petri-Net controller, transitions are controlled by force sensing and discrete event controller schemes. Since state detection by force sensing is not reliable, active controller schemes may become sophisticated in practice and difficult to perform In contrast, an SRCC using passive compliance does not need to

detect states in real time because all possible contact states, uncertainty and constraints for jamming/dead location avoidance have been predicted and included in the compliance design. The need for recognizing intermediate states is not necessary, and constraints for other insertion paths could be determined by a similar procedure.

References

1. Drake, S.H., Watson, P.C., and Simunovic, S.H., 197 7, "High Speed Assembly Using Compliance Instead of Sensory Feedback," *Proc.* of the 7th *Int'l. Symp.* of Industrial Robots.
2. Eppinger, S.D. and Seering, W.P., 19 9 2, "Three Dynamics Problems in Robot Force Control," IEEE Trans. on Robotics and Automation, Vol. 8, No. 6.
3. Kitagaki, K., Ogasawara, T., and Suehiro, T., 1993, "Methods to detect Contact State by Force Sensing in an Edge Mating Task," *Proc.* IEEE *Int'l.* Conf. on Robotics and Automation.
4. McCarragher, B.J. and Asada, H., 1993, "A Discrete Event Approach to the Control of Robotic Assembly Tasks," *Proc.* IEEE Int'l. *Conf.* on Robotics and Automation, Vol. 1.
5. Oh, S. R., Hollis, R.L. and Salsudean, S.E., 1993, "Precision Assembly with a Magnetically Levitated Wrist," *Proc.* IEEE Int'l. *Conf.* on Robotics and Automation, Vol. 1.
6. Ohwovoriole, M.S. and Roth, B., 1981, "An Extension of Screw Theory", Journal of Mechanical Design, Vol. 103.
7. Paetsch, W. and Wichert, G.V., 199 3, "Solving Insertion Tasks with a Multifingered Gripper by Fumbling," *Proc.* IEEE Int'l. Conf. on Robotics and Automation, Vol. 3.
8. Patterson, T. and Lipkin, H., 1990, "A Classification of Robot Compliance," *ASME* Design Technical Conference, Chicago.
9. Riley, F.J., 1983, Assembly Automation, Industrial Press, New York.
10. Simunovic, S., 1975, "Force Information in Assembly Processes," The 5th International Symposium *on* Industrial Robots
11. Sturges, R.H., 1990, "A Quantification of Machine Dexterity Applied to an Assembly Task," Int'l Journal *of* Robotics, Vol. 9. No. 3.
12. Sturges, R.H., and Laowattana, S., 1992, "Virtual Wedging in Three Dimensional Peg Insertion Tasks," Proceedings of the 1992 *IEEE/RSJ* International Conference on *Intelligent Robots and Systems.*

13. Sturges, R.H., and Laowattana, S., 1994, "Polygonal Peg Insertion with Orthogonal Compliance," *The 1994 Japan-USA Symposium on Flexible Automation,* Kobe, Japan.

14. Suehiro, T., and Takase, K., 1990, "Representation and Control on Contact and its Application to Assembly Tasks", *The 5th. International Symposium on Robotics Research,* MIT Press

15. Whitney, D.E., 19 8 2, "Quasi-Static Assembly of Compliantly Supported Rigid Parts," *Journal of Dynamic Systems, Measurement and Control,* Vol. 104.

16. Whitney, D.E., 1987, "Historical Perspective and State of the Art in Robot Force Control." *Int'l Journal of Robotics research,* Vol. 6, No. 1.